Robotics and Computer–Integrated Manufacturing 000 (2017) 1–10

Contents lists available at ScienceDirect

Robotics and Computer–Integrated Manufacturing

journal homepage: www.elsevier.com/locate/rcim

Full length Article

Geometric design optimization of an under-actuated tendon-driven robotic gripper

Huixu Dong[a,*], Ehsan Asadi[a], Chen Qiu[b], Jiansheng Dai[b], I-Ming Chen[a]

[a] Robotic Research Centre, Nanyang Technological University, 50 Nanyang Avenue, 639798 Singapore
[b] Centre for Robotics Research, King's College London, London, United Kingdom

ARTICLE INFO

Keywords:
Geometric design optimization
Stability analysis
Tendon routes
Robotic gripper
Robotic modelling

ABSTRACT

The design optimization of a robotic gripper is of utmost importance for achieving a stable grasp behaviour. This work focuses on analysing the optimal design of an under-actuated tendon-driven robotic gripper with two 3-phalange fingers and a geometric design optimization method is proposed to achieve a stable grasp performance. The problem has twenty-two design variables, including three phalange lengths, three phalange widths, three radii of joint mandrels, a palm width and twelve route variables for allocation of six pulleys. First, the mathematical model between the active and contact forces is expressed in relation to the geometric dimensions of the robotic gripper. Second, the geometric model of transmission characteristics determined by the tendon routes for reducing the resistance is generated. Next, three objective functions and multiple geometric constraints are derived and integrated into two fitness models. Finally, the genetic algorithm is applied to addressing the optimization problem. Practical experiments are performed as well to validate the proposed approach. The approach is universal for optimizing any conventional under-actuated tendon-driven gripper.

1. Introduction

The robotic grippers are required to be all-purpose and capable such as to perform stable grasps and manipulations in unstructured environments. High cost and high complexity design cannot enable robotic grippers to be refined into products. To moderate these limitations, researchers have proposed under-actuated robotic grippers with tendon-driven mechanisms (TDMs) [1–3]. Moreover, two-finger robotic grippers with single actuator are prevalent in research topics and industrial applications because of effective grasping capabilities, the mechanical simplicity and low cost [4,5]. However, robotic gripper design is a very complicated process involving modelling with many parameters [6]. The manipulation performance of an under-actuated gripper significantly depends on the design rather than the control method [7,8]. Thus, it is essential for presenting a novel versatile optimization design for two-finger grippers with TDMs so that the optimized gripper can realizing stable grasps in household and office environments.

A stable grasp is that the grasped object can withstand a range of disturbance from external forces or torques and keep the static equilibrium state [2]. It is well-known that performing a stable grasp is the most important target of gripper design. In order to achieve this target, an under-actuated tendon-driven gripper has to be optimized in the design phase. Specifically, a stable grasp should not result in an ejection phenomenon illustrated by [9]. Since all the joints driven by an active tendon are coupling dependently for each robotic finger, the ratio of the contact forces exerted on an object cannot be changed during the period of run-time. A robotic gripper may eject a grasped object and lead to a roll-back phenomenon on condition that an under-actuated robotic hand is designed incorrectly [10]. Moreover, if the grasped object can withstand a big range of disturbance from the external force/torque, it means the gripper can generate enough forces and torques to resist these disturbances as this equilibrium state is described by the resultant force and torque functions such as $\sum \boldsymbol{F} = 0$ and $\sum \boldsymbol{T} = 0$. The grasping stability is considered as a pre-condition to optimize the dimensions of grippers for the gripper to manipulate objects with a big size range. Indeed, the dimension of a gripper has an important effect on the contact force distribution [11].

A tendon route for an under-actuated robotic gripper with TDMs must be designed and optimized carefully such that forces performed on an object are controlled and the resistance of the restoration motion keeps as low as possible. The tendon-route problem is formulated as an optimization problem of the pulley allocation. The optimization of tendon routes can improve the grasping capability.

This work proposes a new practical design approach to optimizing the dimension parameters of an under-actuated robotic gripper and tendon routes based on genetic algorithm by taking account of geometric constraints. Unlike the other related works, this paper focuses on de-

* Corresponding author.
E-mail address: dong0076@e.ntu.edu.sg (H. Dong).

https://doi.org/10.1016/j.rcim.2017.09.012
Received 4 May 2017; Received in revised form 29 August 2017; Accepted 18 September 2017
Available online xxx
0736-5845/

sign optimization of an under-actuated gripper with TDMs that aims at enhancing the grasping performance for the gripper by adjusting the geometric parameters. The gripper has twenty-two design variables, including three phalange lengths, three phalange widths, three radii of the joint mandrels, a palm width and twelve route variables for allocation of six pullyes. During the course of optimal design, several performance indices are involved, such as the grasping stability, transmission ratio of forces/torques. First, the mathematical model between the active force and the contact forces is extracted to determine the dimension parameters of a gripper. Second, a mathematical model is built to route the tendon with the lowest amount of resistance. Next, two separate optimization processes are presented in detail for the gripper design where three objective functions and multiple geometric constraints are derived and integrated into two fitness models. Finally, the genetic-based optimization algorithm is applied to optimizing the geometric parameters for the stable grasp behaviour and to enhance tendon routes by addressing the layout of pulley allocations. Practical experiments are performed as well to validate the proposed approach.

The rest of the paper is organized as follows. The related works are briefly reviewed in the next section. Design requirements and variables are proposed in Section 3. Section 4 builds the models of force/torque transmission between an actuator and fingers and provides the geometric analysis of the tendon routes. Section 5 constructs the optimization formulation with respect to the models given by the above section. The detail description of the optimization approach and the optimized results are illustrated in Section 6. Section 7 describes the practical grasping experiments. Section 8 gives a conclusion for the proposed framework.

2. Related works

This pioneering works for under-actuated tendon-driven robotic grippers and the corresponding mathematical models are briefly reviewed here. Hirose and Umetani [12] demonstrated the capabilities of an under-actuated tendon-driven robotic hand. The under-actuated mechanism has been utilized in most of robotic hands, such as RTR2 Hand [13], SDK hand [14], and Velo gripper [15], Willow Garage hand [16], robotic gripper with soft surfaces and underactuated joints [17], GR2 Gripper [4], Soft-touch gripper [18]. In addition, there exist many classical publications describing the kinematic and dynamic models regarding an under-actuated tendon-driven gripper. Tsai et al. [19] have established the mathematical model regarding the kinematic structure of tendon-driven robotic mechanisms by the graph theory. The identification and enumeration of the kinematic structure of tendon-driven robotic mechanisms were introduced using a pseudo-triangular structure matrix by [20]. Ou and Tsai [21] proposed a methodology of driving design equations regarding kinematic synthesis of tendon-driven manipulators based on isotropic transmission characteristics. A tendon-driven mechanism (TDM) with active and passive tendons could be grouped into several classes by kinematic analyses, which was presented by Ozawa et al. [22]. However, the prior works do not present the relation between the active force and the contact forces according to the kinematic structure of TDMs and also do not present an approach to calculating the Jacobian of the structure of tendon-driven mechanism using the specific parameters.

The representative optimization methods are given for the under-actuated gripper design. The non-dominated sorting genetic algorithm version II (NSGA-II) is adopted to optimize the force extracted by the robot gripper on the surface of a grasped rigid object in [23]. Datta et al. [24] used multi-objective evolutionary algorithm to optimally calculate the dimensions of links and the joint angle of a robot gripper. Backus and Dollar [25] presented the optimization design approach of an underactuated robotic gripper by comparing the grasping performances of the cylindrical fingers and the single joint fingers. Ciocarlie et al. [26] built a function determining the size range of objects to optimize the links of the gripper. The dimension of robotic gripper was optimized via teaching-learning-based algorithm provided by [11]. The dimension optimization of the robotic gripper was presented by Dollar and Howe [27], depending on the grasping scenarios. Since it is unknown that the number and route of tendons have effects on robotic grasp quality, Inouye et al. [28] utilized a novel computational approach to quantifying grasp quality by optimizing positions of joint centres and a tendon route. Gosselin et al. [29] optimized the route of the active tendon routes by calculating the contact forces for a given configuration. The optimized method, which is based on the line constraint and the plane constraint, was proposed by Treratanakulwong [30]. Ciocarlie et al. [31] provided an approach to optimizing the tendon route such as to make the moment arms be well controlled.

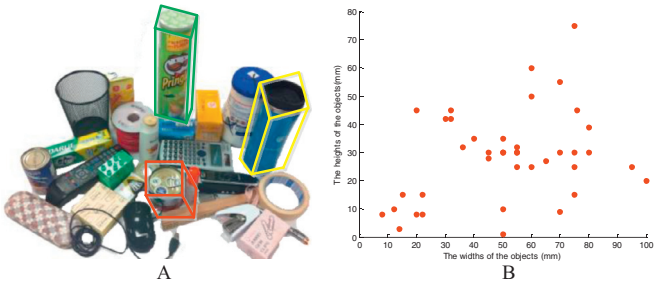

Fig. 1. Objects enclosed by bounding boxes (A) and the dimensions of a set of objects approximated by the dimensions of bounding boxes (B).

3. Desired outcome

3.1. Design requirements

The main design requirements of an under-actuated two-finger gripper with TDMs are set as follows, so as the gripper

(1) can perform a stable grasp.
(2) can perform both the enveloping and fingertip grasp.
(3) includes two 3-phalange fingers with a single actuator.
(4) can return the initial state of the gripper.
(5) can grasp objects with the desired maximum width and a minimum thickness. Considering the robotic application is to manipulate objects, we defined a task of picking items with a maximum width of 100 mm.

The first requirement is the most critical condition of realizing a successful grasp. As for the second and third requirements, the enveloping mode is useful for grasping bigger objects as the enveloping grasp can exert the enclosing force in case of ejecting the object. Besides, the gripper with two 3-phalange fingers provides more contact points than a gripper with 2-phalange fingers for the enveloping grasp. Indeed, the fingertip grasp is a pivotal skill for grippers, since it is performed almost as frequently as a force grasp or an enveloping grasp. The gripper cannot exert an enveloping grasp if the object to be grasped is placed on a flat surface. In this case, the gripper uses the fingertips to pick up a small object. To reduce the resistance of restoration motion [26], the tendon routes must be designed and optimized as for the fourth requirement. Considering the robotic application is to manipulate objects, we defined a task of picking items with different shapes and size but with a maximum width of 100 mm regarding the fifth requirement. In addition, the size of some daily used objects is explored and diverse objects within the desired size range are selected to be used for performance assessment. The dimensions of a set ($n = 40$) of objects, which are used in households and offices [15], are measured approximately by that of the enclosing bounding boxes, as shown in Fig. 1.

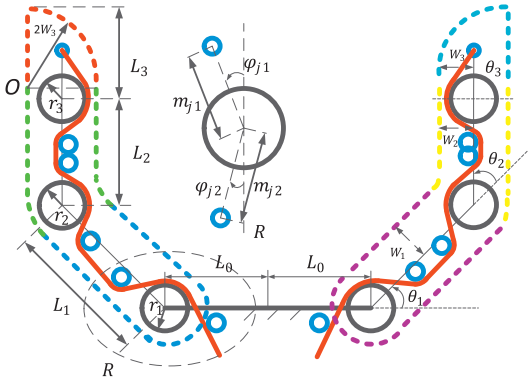

Fig. 2. A schematic of an under-actuated robotic gripper with TDMs.

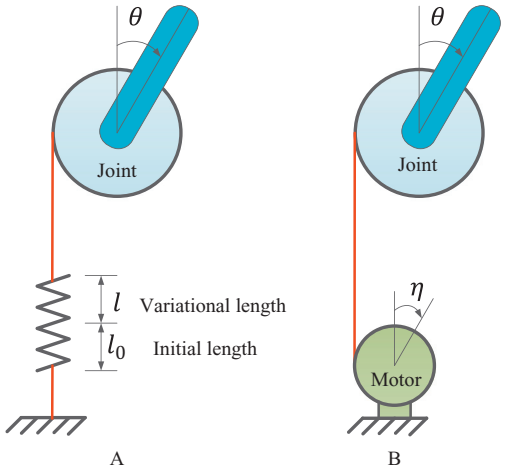

Fig. 3. (A) Passive tendon contacted a spring and (B). Active tendon driven by a motor.

3.2. Design variables

Fig. 2 shows the schematic view of our gripper design. The robotic gripper includes two 3-phalange fingers driven by tendons. For the design of the initial states of three phalanges, we will adopt the expansion model of the reference [15]. θ_1 represents the angle between the first phalange and the palm, and θ_i is the angle between the phalanges i and $i-1$, $i = 2,\ 3$. The initial angles of the three joints are given, such as $\theta_1' = \frac{\pi}{4}$, $\theta_2' = \frac{\pi}{4}$, $\theta_3' = 0$. The fingertip of the third phalange is designed as a curved surface of a quarter of a circle with the radius $2W_3$ and the two end points of the arc are tangent to the two sides of the third phalange, as shown in Fig. 2. For the fingertip grasp, the fingertip with the curved surface will be used frequently. Thus, the radius of the designed fingertip is almost equivalent to the length of the third phalanges. Based on the design requirements, the design variables, which comprises of phalange lengths and the pulley allocation around each joint, are $\omega = (L_1,\ L_2,\ L_3,\ r_1,\ r_2,\ r_3,\ W_1,\ W_2,\ W_3,\ L_0,\ \varphi_{j1},\ \varphi_{j2},\ m_{j1},\ m_{j2})^T$, $j = 1,\ 2,\ 3$, where L_1, L_2, L_3 denote the phalange lengths and L_0 is the half width of the palm; r_1,r_2, r_3 denote the radius of the three joints, respectively; W_1, W_2, W_3 are the half widths of the first, second and third phalange. The pulley positions used for guiding the tendons can be illustrated by the polar coordinates φ_{j1}, m_{j1} and φ_{j2}, m_{j2} whose centre is that of the joint mandrel j, as shown in Fig. 2. Specifically, $\varphi_{j1,\,2}$ represents the angles with the positive direction pointed by an arrow mark between the centre axis of the phalanx $L_{j,\,j-1}$and the contacting line from the centre of joint j to the pulley for guiding a tendon mounted on the phalanx $j,\ j-1$, correspondingly; $m_{j1,\,2}$ denotes the distance between the centre of the joint j and the pulley attached on the phalanx $j,\ j-1$, respectively.

4. Problem modelling

The force/torque transmission from the actuator to robotic fingers [24] determines the grasping forces/torques that exert an object. The models of force/torque transmission are built for optimizing the dimensions of robotic fingers, to a lesser extent, to reduce the subjective considerations from the topology of anthropomorphic hand. Moreover, the geometric model for pulley allocations is constructed to optimize tendon routs for relieving the resistance of restoration motion.

4.1. The model of force/torque transmission

4.1.1. The transmission of tension forces and joint torques

To obtain the relation of the tendon tension force and the joint torque, we can establish the kinematics of tendon-driven mechanism [22]. There exist two tendon-driven types, including the passive tendon with a spring and the active driven by an actuator in Fig. 3.

Depending on the kinematic relation between the tendon extension $l \in \mathbb{R}^L$ and the variables such as the joint angle vectors $\boldsymbol{\theta}$ and the actuator rotation angle vectors $\boldsymbol{\eta}$ in Fig. 3, the tendon transmission mechanism can be described as

$$l = l(\boldsymbol{\theta}, \boldsymbol{\eta}, l_0) = \begin{bmatrix} l_a(\boldsymbol{\theta}, \boldsymbol{\eta}) \\ l_p(\boldsymbol{\theta}, l_0) \end{bmatrix}, \tag{1}$$

where $l_a(\boldsymbol{\theta}, \boldsymbol{\eta})$ and $l_p(\boldsymbol{\theta}, l_0)$ are the extensions for active tendon parameters $\boldsymbol{\theta}, \boldsymbol{\eta}$ and passive tendon parameters $\boldsymbol{\theta}, l_0$, respectively. Specifically, $\boldsymbol{\theta} = (\theta_1,\ \theta_2, \cdots,\ \theta_N) \in \mathbb{R}^N$ and $\boldsymbol{\eta} = (\eta_1,\ \eta_2, \cdots,\ \eta_A) \in \mathbb{R}^A$. L, N and A represent the number of tendons, joints and actuators, correspondingly. l_0 denotes the initial extension for the passive tendon. Moreover, setting $\boldsymbol{J}_k$ to be a Jacobian matrix that maps the joint angle velocity vector $\dot{\boldsymbol{\theta}}$ to the tendon extension rate $\dot{l}$. The derivative of the tendon extension regarding time can be provided by

$$\dot{l} = \begin{bmatrix} \dot{l}_a(\boldsymbol{\theta}, \boldsymbol{\eta}) \\ \dot{l}_p(\boldsymbol{\theta}, l_0) \end{bmatrix} = \boldsymbol{J}_k \dot{\boldsymbol{\theta}} + \begin{bmatrix} R_a \\ 0 \end{bmatrix} \dot{\boldsymbol{\eta}} \tag{2}$$

with

$$\boldsymbol{J}_k = \begin{bmatrix} \boldsymbol{J}_a \\ \boldsymbol{J}_p \end{bmatrix}$$

where $\boldsymbol{J}_a$ and $\boldsymbol{J}_p$ are the corresponding Jacobian matrixes, and $\boldsymbol{R}_a$ is the diagonal matrix whose diagonal elements are the pulley radius connected with actuators. Then, depending on the principle of virtual work, the next equation is obtained:

$$\boldsymbol{\tau} = -\boldsymbol{J}_k^T \boldsymbol{F}_t. \tag{3}$$

Since the tension force is just considered, the negative sign is referred in the above equation. $\boldsymbol{F}_t$ represents the vector of tendon tension force, which is constantly positive since all the tendons cannot generate negative tension force. $\boldsymbol{\tau}$ is the joint torque vector.

4.1.2. The transmission of contact forces and joint torques

The idlers are applied to compress tendons, which allow the tendons to be in contact with mandrels during the period of joint rotation, such as to ensure the moment arm of the joint torque is the radius of joint. A torque spring used in a practical robotic finger is equivalent to two linear springs for simplifying the model, as shown in Fig. 4(A). According to this equivalent model, a finger has seven tendons in the desired design, including one active tendon and six passive ones in Fig. 4(B). Referring to [2,20], all the radii of joints are supposed to be identical in order to simplify the model of the tendon-driven mechanism. However, in this paper, the specific radius values are given to calculate the equation of each driven tendon. The radii of joint pulleys are assumed to be r_1, r_2 and r_3 .The mapping Jacobian matrix $\boldsymbol{J}_k$ is obtained based on the following principle. The elements of the mapping Jacobian matrix are determined by the rotational direction of the joint axes and the tendon route. But in

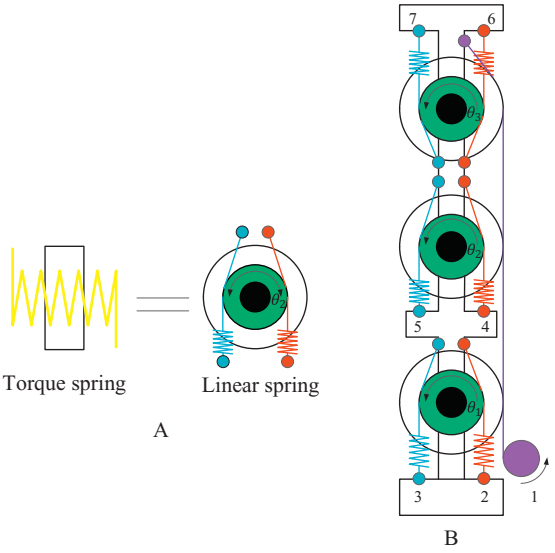

Fig. 4. Schematic diagram of the tendon-driven mechanism regarding an under-actuated finger. The purple circle on the right represents an actuator. (For interpretation of the references to colour in this figure legend, the reader is referred to the web version of this article.)

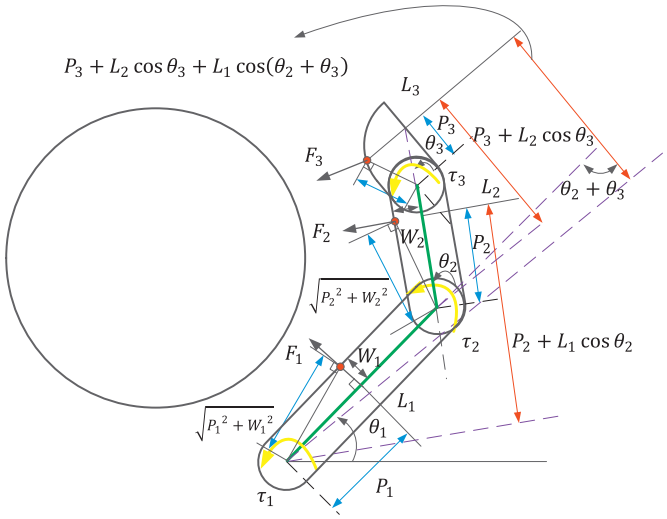

Fig. 5. The schematic diagram of the geometric model for the enveloping grasp. The red dots represent the contact points.L_i is the length of the phalange *i*; P_i denotes the distance from the joint *i* to the contact point;W_i indicates the half width of the phalange *i*; The contact force is F_i for the joint *i*; τ_i is the torque of the joint *i*, $i = 1, 2, 3$. (For interpretation of the references to colour in this figure legend, the reader is referred to the web version of this article.)

fact, the elementary line transformation of the mapping Jacobian matrix has no effect on the function of the mechanism. That is, the mapping Jacobian matrix $\boldsymbol{J}_k$ of elementary transformation is equivalent. Thus, the definition of direction for the joints makes no difference to the tendon-driven mechanism. For instance, the positive direction of rotational joint is defined to be pointing out of the paper, the mapping Jacobian matrix J_k is described as follows:

$$\boldsymbol{J}_k{}^T = \begin{bmatrix} r_1 & r_1 & -r_1 & 0 & 0 & 0 & 0 \\ r_2 & 0 & 0 & r_2 & -r_2 & 0 & 0 \\ r_3 & 0 & 0 & 0 & 0 & r_3 & -r_3 \end{bmatrix} \tag{4}$$

The tendon tension force $\boldsymbol{F}_t$ is presented by

$$\boldsymbol{F}_t = \begin{bmatrix} F_{t1} \\ F_{t2} \\ F_{t3} \\ F_{t4} \\ F_{t5} \\ F_{t6} \\ F_{t7} \end{bmatrix} = \begin{bmatrix} F_a \\ k_1\Delta\theta_1 \\ -k_1\Delta\theta_1 \\ k_2\Delta\theta_2 \\ -k_2\Delta\theta_2 \\ k_3\Delta\theta_3 \\ -k_3\Delta\theta_3 \end{bmatrix} \text{ with } \begin{bmatrix} \Delta\theta_1 \\ \Delta\theta_2 \\ \Delta\theta_3 \end{bmatrix} = \begin{bmatrix} \theta_1 - \frac{\pi}{4} \\ \theta_2 - \frac{\pi}{4} \\ \theta_3 \end{bmatrix} \tag{5}$$

where $F_{ti}(i = 1, 2, \cdots, 6, 7)$ represents the tension force of each tendon. The assumption is that the stiffness of two springs attached on each joint is identical. $k_i(i = 1, 2, 3)$ are the stiffness of linear springs for the joint 1, 2, and 3, respectively. $\boldsymbol{F}_a$ indicates the tension force of the active tendon and $\Delta\theta_i(i = 1, 2, 3)$ are the variations of joint angles with respect to the initial values $\frac{\pi}{4}$, $\frac{\pi}{4}$, 0 for θ_1, θ_2 and θ_3, correspondingly. From Eq. (3), we can obtain the following equation:

$$\boldsymbol{\tau} = \begin{bmatrix} \tau_1 \\ \tau_2 \\ \tau_3 \end{bmatrix} = -\begin{bmatrix} F_a r_1 + 2k_1\Delta\theta_1 r_1 \\ F_a r_2 + 2k_2\Delta\theta_2 r_2 \\ F_a r_3 + 2k_3\Delta\theta_3 r_3 \end{bmatrix}. \tag{6}$$

4.1.3. The model of the contact forces

The active forces, which are generated by the actuator and transmitted by the phalanges, will be used in the optimization procedure. In practical grasping applications, sometimes the palm of the gripper also provides a supporting force to the grasped object. However, a supporting force belongs to a passive force and will not be optimized.

The presented gripper is a planner mechanism with a single actuator. Because of the symmetry, we merely focus on a half of this mechanism that is made up of three phalanges and three joints, as illustrated in Fig. 5. According to the principle of virtual work, the equilibrium equation of the *i*th phalanx can be provided by

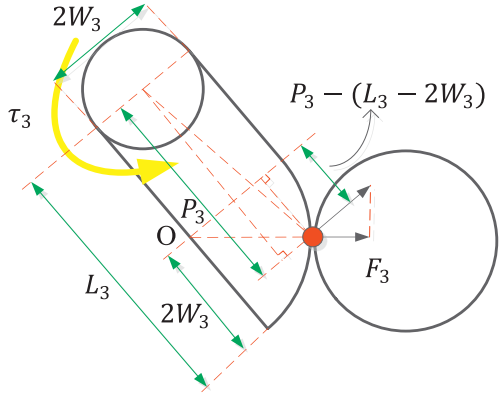

Fig. 6. The schematic diagram of geometric model for the fingertip grasp. The red dot represents the contact point. *O* is the center of the curved surface of the fingertip whose radius is $2W_3$. (For interpretation of the references to colour in this figure legend, the reader is referred to the web version of this article.)

$$\boldsymbol{\tau} = \boldsymbol{J}_i^T \boldsymbol{F}_i \tag{7}$$

where $\boldsymbol{J}_i$ is Jacobian matrix of the finger with three phalanges, and $\boldsymbol{F}_i$ denotes the force of the i^{th} contact point regarding the fixed palm frame of reference; $\boldsymbol{\tau}$ is the *i*th joint torque of the under-actuated robotic finger. The geometric approach is applied to achieving the Jacobian matrix $\boldsymbol{J}_i$ that maps the contact force $F_i(i = 1, 2, 3)$ exerted on a grasped object to the joint torque τ. M_1, M_2 and M_3 are the moment arms of the torque τ_1, τ_2, τ_3, respectively. In Figs. 5 and 6, the magnitude of the applied torque τ_3 is presented as:

$$|\tau_3| = |F_3 M_3|, \tag{8}$$

However, there are two frequently-used grasping modes for the gripper such as the enveloping grasp and the fingertip grasp. The flat plane part of the third phalange will be blocked by the second phalange when the third joint does the flex motion due to the high ratio of the radius of the curved surface to the length of the third phalange. During the grasping period, the contact point of the third phalange with the grasped

object is on the curved surface rather than the flat plane, as illustrated in Fig. 6.

When the contact point is on the curved surface in Figs. 5 and 6, the moment arm depending on the geometric analysis is described as follows

$$M_3 = \frac{{P_3}^2 + \left(\sqrt{(2W_3)^2 - \left[P_3 - (L_3 - 2W_3)\right]^2} - W_3\right)^2}{P_3}.$$

The torques τ_2 and τ_1, which are illustrated in Fig. 5, can be provided as listed below

$$\tau_2 = F_2 M_2 + F_3\left(P_3 + L_2\cos\theta_3\right), \tag{9}$$

$$\tau_1 = F_1 M_1 + F_2\left(P_2 + L_1\cos\theta_2\right) + F_3 P_A \tag{10}$$

with $P_A = P_3 + L_2\cos\theta_3 + L_1 cos(\theta_2 + \theta_3)$ and $M_i = \frac{P_i^2 + W_i^2}{P_i}$, $i = 1, 2$.

Furthermore, the transpose of the Jacobian matrix can be obtained as follows

$$\boldsymbol{J}_i^T = \begin{bmatrix} M_1 & P_2 + L_1\cos\theta_2 & P_A \\ 0 & M_2 & P_3 + L_2\cos\theta_3 \\ 0 & 0 & M_3 \end{bmatrix}. \tag{11}$$

The phalanges of the gripper are regarded as rigid bodies. Each phalanx does not have more than one contact point with the grasped object. Due to the low speed movement and the light quality of the fingers compared with F_a, the dynamic properties of the gripper will not be analyzed and the grasp maintains the static equilibrium [32]. Thus, combined Eqs. (6) and (7), the contact force F_1, F_2, F_3 are described by

$$F_3 = \frac{1}{M_3}\left(F_a r_3 + 2k_3\Delta\theta_3 r_3\right), \tag{12}$$

$$F_2 = \frac{1}{M_2}\left[F_a r_2 + 2k_2\Delta\theta_2 r_2 - F_3\left(P_3 + L_2\cos\theta_3\right)\right], \tag{13}$$

$$F_1 = \frac{1}{M_1}\left(F_a r_1 + 2k_1\Delta\theta_1 r_1 - F_2 P_B - F_3 P_A\right) \tag{14}$$

with $P_B = P_2 + L_1\cos\theta_2$.

The spring stiffness is not only sufficiently strong to keep the phalanges return the initial positions overcoming the resistance without the actuator forces but also as low as possible in order to relieve the actuated force consumption. As a standard mechanical part, the stiffness k_i is a constant. Since the actuated force F_a is far larger than the spring tension force F_t, the contact force can be simplified as follows

$$F_3 = \frac{1}{M_3}F_a r_3 \tag{15}$$

$$F_2 = \frac{1}{M_2}\left[F_a r_2 - F_3\left(P_3 + L_2\cos\theta_3\right)\right], \tag{16}$$

$$F_1 = \frac{1}{M_1}\left[F_a r_1 - F_2 P_B - F_3 P_A\right] \tag{17}$$

4.2. The geometric model for pulley allocations

4.2.1. Force transmission efficiency for a tendon through joints

Due to the friction, the tendon tension force cannot be transmitted totally when the tendon wraps the joint mandrel. The enveloping angle is defined as the central angle that is made up of the centre of the joint and two radii the two end tangent points formed a tendon wrapping a joint mandrel, as shown in Fig. 7. Let an enveloping angle α approach an infinitesimal angle θ that is the equilibrium point. The tangent and normal equilibrium equations are provided as follows

$$\left(F_{tan} + dF_{tan}\right)\sin\frac{d\theta}{2} + F_{tan}\sin\frac{d\theta}{2} = dN, \tag{18}$$

$$\left(F_{tan} + dF_{tan}\right)\cos\frac{d\theta}{2} - F_{tan}\cos\frac{d\theta}{2} = \mu dN \tag{19}$$

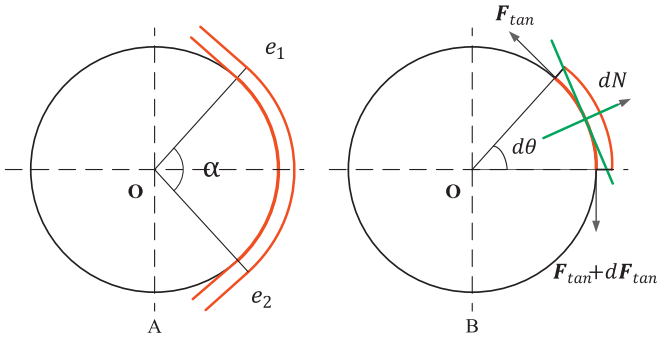

Fig. 7. Schematics of the enveloping angle (A) and forces exerting a surface along the tangent direction (B). e_1 and e_2 represent the two end tangent points of a tendon wrapping the mandrel.

where N represents the supporting force from the object compressed against the surface of the joint mandrel, while μ is the friction coefficient between a tendon and the object. Then, as θ is a tiny value, $\sin\frac{d\theta}{2} \approx \frac{d\theta}{2} \approx 0$, $\cos\frac{d\theta}{2} \approx 1$. Substituting these two equations into (18) and (19), we can obtain the following equations:

$$F_{tan}d\theta = dN, \tag{20}$$

$$dF_{tan} = \mu dN. \tag{21}$$

Thus, the function equation can be expressed as follows:

$$\frac{dF_{tan}}{F_{tan}} = \mu d\theta. \tag{22}$$

Integration of both sides yields

$$\int_{F_{resist}}^{F_{tension}} \frac{dF_{tan}}{F_{tan}} = \int_0^{\alpha} \mu d\theta. \tag{23}$$

Thus,

$$F_{external} = F_{resist}e^{\mu\alpha}, \tag{24}$$

where $F_{external}$ denotes the contact tangent force generated by the active tendon tension force and F_{resist} expresses the resisting force for keeping the current state.

Based on the above derivation, we can come to a conclusion. Specifically, when the friction coefficient μ is a constant value and the resisting force, F_{resist}, is a fixed value, the larger the enveloping angle α is, the more the capability of resisting the tendon tension force, $F_{external}$ is. Finally, the efficiency η of the force transmission for the tendon wrapping the mandrel is

$$\eta = \frac{\boldsymbol{F}_{resist}}{\boldsymbol{F}_{external}} = \frac{1}{e^{\mu\alpha}}. \tag{25}$$

4.2.2. The geometric model determining the tendon routes

The tendon routes can be guided by the joint mandrel and pulleys. The geometric parameters of determining the tendon routes, m_{j1}, φ_{j1}, m_{j2}, φ_{j2}, $(j = 1, 2, 3)$, are illustrated schematically in Fig. 8.

As the capability of the springs is equivalent to that of the passive tendons for a robotic finger, a tendon referred in the latter sections is an active tendon rather than a passive tendon. The tendon is the unique component attached to the motor and controlled at runtime. The joint mandrels and pulleys can lead the tendon to slide through a series of the route points such as to change the direction of the active tension force and determine the joint torques generated by the tendon. The moment arm regarding the joint mandrel equals the radius of the joint mandrel r_j if and only if the tendon is touching the mandrel. Therefore, the moment arm must be first confirmed and then determines the torque in real time. The critical condition, which allows the tendon to touch the joint mandrel all the time during the rotational motion of joint, is that the contacting line of the pulleys on the two sides of the joint mandrel is

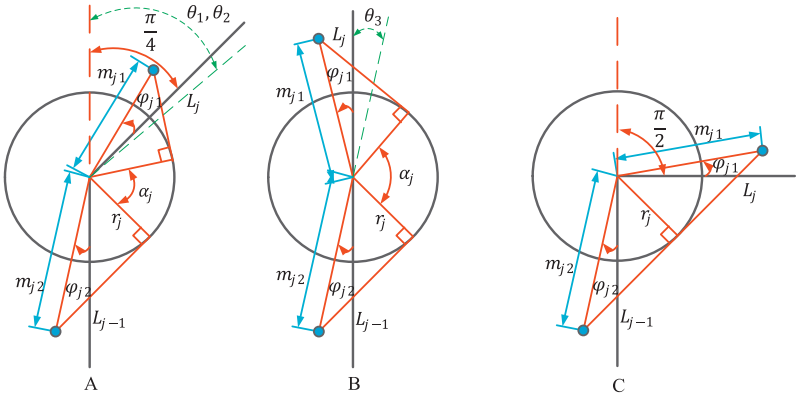

Fig. 8. (A) Tendon routes of the first and second joints: The two phalanges for the first or second joint form the interaction angle $\frac{3}{4}\pi$; (B) The third joint at the initial position: the distal and middle phalanges configure the angle π; (C) The state of the maximum flex angle for all the joints which is $\frac{1}{2}\pi$. α_j is the tendon enveloping when the tendon wraps around the joint mandrel j. The blue dots represent the pulleys. The green dashed lines represent the position of the phalange L_j when the phalange L_j rotates relative to the phalange L_{j-1}. θ_j represents the intersection angle between the phalanges L_j and L_{j-1}. (For interpretation of the references to colour in this figure legend, the reader is referred to the web version of this article.)

tangent to the mandrel when the two phalanges form the maximum flex angle $\Delta\theta_{imax}(\Delta\theta_i = \theta_i - \frac{\pi}{4}$ *or* θ_i, $\Delta\theta_{imax} = \frac{\pi}{4}$ *or* $\frac{\pi}{2})$, as shown in Fig. 8.

Based on the derivations in the above part, the enveloping angle α_j determines the efficiency of the force transmission for the tendon wrapping the mandrel if the coefficient of friction is a constant. When the phalanges can be back to the initial states without the active force, the springs must overcome the resistance from the tendon routes. In order to increase the force transmission efficiency, the enveloping angle α_j at the initial position should decrease suitably under the condition of tendon touching the joint mandrel. Thus, the enveloping angle α_j is provided as:

$$\alpha_j = \varepsilon - \left(\cos^{-1}\frac{r_j}{m_{j1}} - \varphi_{j1} + \cos^{-1}\frac{r_j}{m_{j2}} - \varphi_{j2}\right) \tag{26}$$

where ε represent the initial intersection angle between the two phalanges. In detail, ε is $\frac{3}{4}\pi$ for the first and second joints and ε is evaluated by $\frac{3}{4}\pi$ regarding the third joint. θ_1, θ_2

5. Optimization formulation

5.1. Objective functions

5.1.1. The objective functions for the dimension optimization

Having the relation between contact forces and dimension parameters, the two criterions of evaluating the grasping stability are described based on the sum of the grasping forces and the distribution of contact forces.

The first objective function (Eq. (27)) is written as the sum of grasping forces. A bigger contact force means the grasped object can withstand a stronger external disturbance for improving the grasping stability. The maximization of this objective ensures that the gripper can realize a stable grasp readily.

$$\delta_1 = F_1 + F_2 + F_3, \tag{27}$$

The second objective function (Eq. (28)) is the magnitude of difference values among the contact forces. There should be not the big difference among the contact forces in case of ejecting an object [9,10]. The minimization of this objective will ensure that the exerted forces are almost uniform. For describing this metric, we use the function δ_2 to build the expressions as follows

$$\delta_2 = \left(\bar{F} - F_1\right)^2 + \left(\bar{F} - F_2\right)^2 + \left(\bar{F} - F_3\right)^2 \tag{28}$$

with

$$\bar{F} = \frac{F_1 + F_2 + F_3}{3}$$

where δ_1 represents the total contact force and δ_2 donates the discrete magnitude for the contact forces.

If a phalange does not include a contact point with the grasped object, the force from this phalange will be zero. For example, the second and third phalanges will not exert the forces for the fingertip grasp, that is, F_1 and F_2 are zeros.

5.1.2. The objective function for the tendon routes

The object function (Eq. (26)) is the enveloping angle for the active tendon wrapping the mandrel. We will allow this objective to be minimum to improve the force transmission efficiency. The object function τ_j is illustrated as follows

$$\tau_j = \alpha_j \tag{29}$$

5.2. Geometric constraints

5.2.1. Constraints for the dimension optimization

(1) We refer to the human finger and the length ratio among phalanges [33] for allowing the geometric dimensions to be within a suitable range. All the geometric dimensions must fall into the required ranges according to Table 1.

(2) The geometric bounds of the rotation angles of the joints are given as follows (in radian),

$$\frac{\pi}{4} \le \theta_1 \le \frac{\pi}{2}$$

$$\frac{\pi}{4} \le \theta_2 \le \frac{\pi}{2}$$

$$0 \le \theta_3 \le \frac{\pi}{2}.$$

(3) The length of the phalanx $L_i(i = 1, 2, 3)$ must be larger than the contact position $P_i(i = 1, 2, 3)$. The function g_i represents the difference between these two parameters. Specifically,

$$g_1 = P_1 - L_1 \le 0;$$

$$g_2 = P_2 - L_2 \le 0;$$

$$g_3 = P_3 - L_3 \le 0.$$

Thus, the formula $max(0, g_i)$ can be described by

$$max(0, g_i) = \begin{cases} 0, & g_i \le 0 \\ g_i, & g_i > 0 \end{cases}.$$

(4) The fingertip is always used for manipulating small objects. The fingertip accounts for the large ratio of all the third phalange in volume [34].We set the ratio of the radius of the fingertip to the length of

Table 1
Dimension constraints for robotic gripper.

Geometric dimension(mm)	L_1	L_2	L_3	r_1	r_2	r_3	$2W_1$	$2W_2$	$2W_3$
Lower limit(mm)	40	25	15	6	6	6	10	10	10
Upper limit(mm)	60	40	25	15	15	15	20	20	20

Table 2
The first joint: ranges of the parameters.

Route parameters	Lower limit	Upper limit
m_{11}(mm)	$max(15, r_1)$	$max(15, 0.5L_1)$
φ_{11}(rad)	0	0.25π
m_{12}(mm)	$max(15, r_1)$	$max(15, 0.5L_0)$
φ_{12}(rad)	0	0.25π

Table 3
The second joint: ranges of the parameters.

Route parameters	Lower limit	Upper limit
m_{21}(mm)	$max(10, r_2)$	$max(15, 0.5L_2)$
φ_{21}(rad)	0	0.25π
m_{22}(mm)	$max(10, r_2)$	$max(15, 0.5L_1)$
φ_{22}(rad)	0	0.25π

Table 4
The third joint: ranges of the parameters.

Route parameters	Lower limit	Upper limit
m_{31}(mm)	$max(10, r_3)$	$max(15, L_3)$
φ_{31}(rad)	0	0.25π
m_{32}(mm)	$max(10, r_3)$	$max(15, 0.5L_2)$
φ_{32}(rad)	0	0.25π

the third phalange as a geometric constraint for the optimization procedure.

$$0.7 \le \frac{2W_3}{L_3} \le 1.$$

We use the functions γ_1 and γ_2 to describe these constraints as follows

$$\gamma_1 = \begin{cases} 0, & 0.7L_3 - 2W_3 \le 0 \\ 0.7L_3 - 2W_3, & 0.7L_3 - 2W_3 > 0 \end{cases}.$$

$$\gamma_2 = \begin{cases} 0, & 2W_3 - L_3 \le 0 \\ 2W_3 - L_3, & 2W_3 - L_3 > 0 \end{cases}.$$

(5) The distance P_3 between the contact point and the third joint for the third phalanx L_3 must be larger than $(L_3 - 2W_3)$. The following function ϵ represents the difference between P_3 and $(L_3 - 2W_3)$,

$$\epsilon = P_3 - \left(L_3 - 2W_3\right).$$

Hence, the constraint formula $\zeta(\epsilon)$ is presented as

$$\zeta(\epsilon) = \begin{cases} \epsilon^2, & \epsilon \le 0 \\ 0, & \epsilon > 0 \end{cases}.$$

(6) The width of the phalange i must be not less than the diameter of the joint i such that the joint mandrel cannot be exposed outside of the fingers. We build two functions, such as $min(W_1, W_2, W_3)$ and $max(r_1, r_2, r_3)$, to describe the relation between the width of the phalange and the radius of the joint mandrel. The function $min(W_1, W_2, W_3)$ obtains the minimum value of W_1, W_2, W_3 and the function $max(r_1, r_2, r_3)$ gets the maximum value of r_1, r_2, r_3.The geometric constraints are provided as follows:

$$min(W_1, W_2, W_3) \ge max(r_1, r_2, r_3).$$

5.2.1. Constraints for the optimization of tendon routes

(1) According to the geometric constraints in Fig. 8, the initial geometric constraints for the tendon touching the joint mandrel can be given by

$$h = \frac{\pi}{2} - \left(\sin^{-1}\frac{r_j}{m_{j1}} + \varphi_{j1} + \sin^{-1}\frac{r_j}{m_{j2}} + \varphi_{j2}\right) \le 0.$$

(2) Geometric constraints for the allocation parameters of the pulleys are provided by Tables 2, 3 and 4. The function $max(a, b)$ is used in getting the maximum of a and b.

6. Optimization procedure and results

6.1. Optimization method

Since a function with many variables is difficult to isolate each parameter and get the derivation, Genetic Algorithm (GA) [35] is adopted in optimizing the geometric dimensions of a robotic gripper and pulley allocations for guiding the tendon routes.

6.2. Fitness function constructions

6.2.1. Fitness function for the dimension optimization

The first fitness function $f_{dimension}$ is constructed based on the two objective functions under the condition of some constraints. For an optimization method, GA itself has no capability to handle the constraints. When dealing with the functional optimization with constraints using GA, we can make it be the problem without constraints. The lower and upper limits of the geometric dimensions can be considered during the period of encoding the chromosomes, while a penalty function p is introduced in a fitness function such that the optimization with constraints is transferred to the corresponding optimization that does not contain constrains but the penalty function p, to deal with the equations and inequality constraints. In order to ensure a stable grasp and resist to a large external disturbance, the total force δ_1 tends to be as high as possible. As to the second criteria δ_2, the contact forces should be well distributed among the phalanges, which come close to be uniform, to avoid large local forces exerted on a grasped object. Therefore, the second criteria δ_2 should be as small as possible, in other words, $\frac{1}{\delta_2}$ leans to be larger. Finally, to achieve the maximum objective value, the fitness function with the geometric constraints is defined by

$$f_{dimension} = \left(\delta_1 + \frac{k}{1+\delta_2} + p\right)\delta_3, \tag{30}$$

with $p = c\sum_{1}^{n}(max(0, g_i) + \zeta(\epsilon) + \gamma_1 + \gamma_2)^2$ and $\delta_3 = 1$ *or* 0. If the grasp is successful, δ_3 becomes 1 and otherwise 0. Since the actuated force F_a is a constant in the fitness function and different from the reference [24], it has no effect on the change amount of $f_{dimension}$ and will not be optimized. The formula $\frac{1}{\delta_2}$ is amplified k times to compensate the difference of δ_1 and $\frac{1}{\delta_2}$ in the numeral magnitude. In this work, the actuator in the gripper prototype can execute a known force to the active tendon based on the positive transmission mechanism. As the difference of δ_1 and $\frac{1}{\delta_2}$ is about 1000 in numeral magnitude, k can be specified 1000. In terms of the second item in Eq. (30), the formula $(1 + \delta_2)$ cannot enable the denominator to be zero. c is the penalty coefficient. In general, c is one order of magnitude bigger than $f_{dimension}$ [35] and it is assigned to be 1000. Specifically, satisfying the constraints, the value of the fitness function becomes larger. In contrast, if violating the constraints, the value of the

Table 5
Geometric dimensions, average optimized results and final values.

Geometric dimensions(mm)	L_1	L_2	L_3	$2r_1$	$2r_2$	$2r_3$	$2W_1$	$2W_2$	$2W_3$
Average optimized results(mm)	54.78	33.81	25.22	15.74	7.73	16.44	17.82	16.97	18.32
Final values(mm) [a]	54.8	33.8	25.2	15.7	7.7	16.4	17.8	17.0	18.3

[a] The final values are adopted in making the gripper.

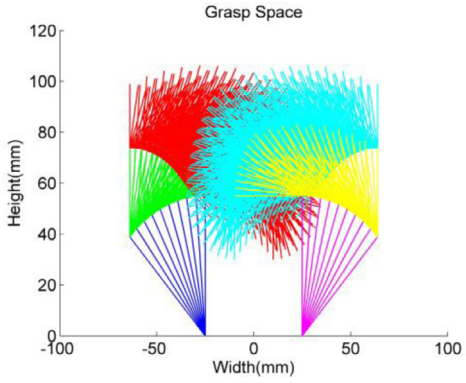

Fig. 9. The grasping space of gripper with two 3-link fingers under different angle combinations.

fitness function greatly decreases due to the large penalty coefficient so that the genes cannot pass on the next generation.

6.2.2. *Fitness function for the optimization of pulley allocation*

We can build the second fitness function $f_{routing}$ to explore the minimum fitness value by the object function τ_j with the corresponding constraints. The fitness function $f_{routing}$ with respect to the tendon routes is defined as follows

$$f_{routing} = \alpha_j + ch^2 \tag{31}$$

with $c = 1000$.

6.3. *Optimized results*

The populations are generated by a random method. For ensuring the generality of the solution, we adopt the different number of the initial population such as 20, 25, 30, 35 and 40. In this work, the single-point crossover operator is used for making the genes from the two parents to be exchanged. As for a mutation operator, it can maintain the genetic diversity and the probability of mutation is set 0.01. Since it is difficult to determine the convergence of GA, the general method is to configure the number of evolutional generation. The number of the evolutional generations is confirmed to be 100 as the stop criteria experimentally. All the setting GA parameters will be applied to optimizing the dimensions of the gripper and tendon routes.

6.3.1. *Optimized results of the geometric dimensions*

The fitness function includes the second and third joint angle variables. Since the joint angles have different combination configurations for different grasps, these variables do not need to be optimized and can be given constants. The second joint angle (θ_2), which is between $\frac{\pi}{4}$ and $\frac{\pi}{2}$, is sampled every $\frac{\pi}{24}$. While the sampled step increment of the third interaction angle (θ_3) within between 0 and $\frac{\pi}{2}$ is also $\frac{\pi}{24}$. Thus, there are 72 combinations (θ_2, θ_3) of different angles in total. The grasp space is illustrated by different angle combinations in Fig. 9. For each angle combination (θ_2, θ_3), the optimization procedure is performed and finally, we adopt the average values of optimized parameters of 72 times to be the optimized results, as shown in Table 5. We will adopt the approximate values of the optimized results in fabricating the robotic gripper.

Table 6
The first joint: the optimized results.

Route parameter	m_{11}(mm)	φ_{11}(rad)	m_{12}(mm)	φ_{12}(rad)
Optimization parameters	24.797	0.58	17.35	0.052
Final values	24..8	0.6	17.4	0

Table 7
The second joint: the optimized results.

Route parameter	m_{21}(mm)	φ_{21}(rad)	m_{22}(mm)	φ_{22}(rad)
Optimization parameters	16.557	0.529	24.83	0.426
Final values	16.6	0.5	24.8	0.4

Table 8
The third joint: the optimized results.

Route parameter	m_{31}(mm)	φ_{31}(rad)	m_{32}(mm)	φ_{32}(rad)
Optimization parameters	16.61	0.025	17.867	0.445
Final values	16.6	0.0	17.9	0.4

According to the geometric relation in Fig. 10. The width of the maximum stretching state d for the gripper can be determined as follows

$$d = 2L_0 + 2L_1 \cos\theta_1' - 2W_3. \tag{32}$$

The maximum desired width of the grasped object w_{obj} ($w_{obj} = 100\ mm$) must satisfy the following in equation

$$w_{obj} \le d.$$

Thus, the palm width of the gripper $2L_0$ can be confirmed.

6.3.2. *Optimized results of tendon routes*

The tendency of the fitness values with respect to the different generations is shown in Figs. 11, 12 and 13, for the optimization of tendon routes. The optimized results of the geometric parameters of determining the tendon routes, such as m_{j1}, φ_{j1}, m_{j2}, φ_{j2} previously introduced in Fig. 8, are given in Tables 6, 7, and 8 for the three joints. Moreover, the hardware fabrication is considered in designing the robotic phalanges and thus, the geometric parameters adopted can be merely approximate values. Tables 6, 7 and 8 also present the final parameters adopted in making the robotic finger, correspondingly.

7. Experimental results

By adopting the final geometric parameters (dimensions and tendon routes) obtained by the proposed method, as shown in Tables 5, 6, 7, and 8, the gripper design is finalized for manufacturing and a prototype is fabricated accordingly, as shown in Fig. 14.

The assessment method previously proposed in [25] for a successful grasping is used in our grasping experiments. An object is put in the centre of the workspace. The grasp is considered a success, if the gripper could grip the object and carry it till the object loses contact with the table surface, while the object remains between fingers for at least 10 s after the gripper is moved up about 15 cm. The gripper releases the grasped object when the tendon tension force is lost. In our experiment, the gripper was applied to grasping 40 objects, which were found in household and office environments, with the size range from the maximum gripper span to a business card. Experimental results indicate that

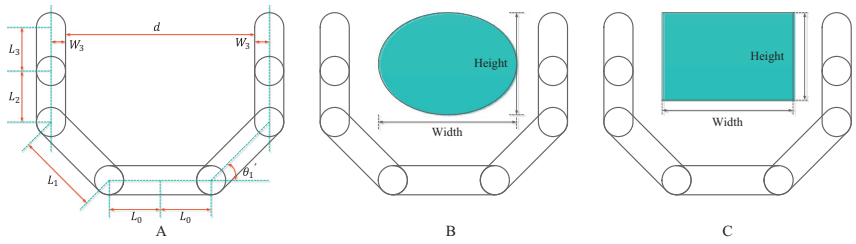

Fig. 10. The initial state of the gripper to grasp an object(A).The gripper grasps the elliptical object(B) and the rectangle object(C).

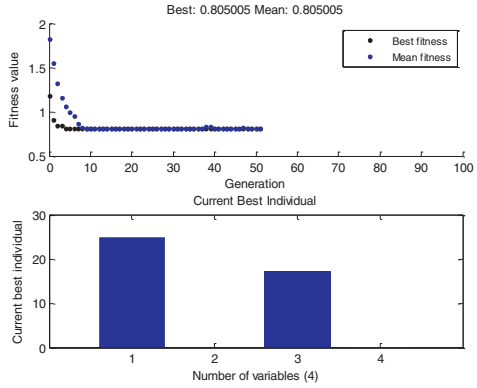

Fig. 11. The first joint: the objective values of different generations and the current optimized values.

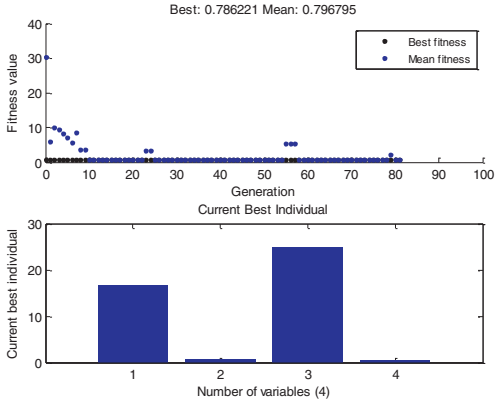

Fig. 12. The second joint: the objective values of different generations and the current optimized values.

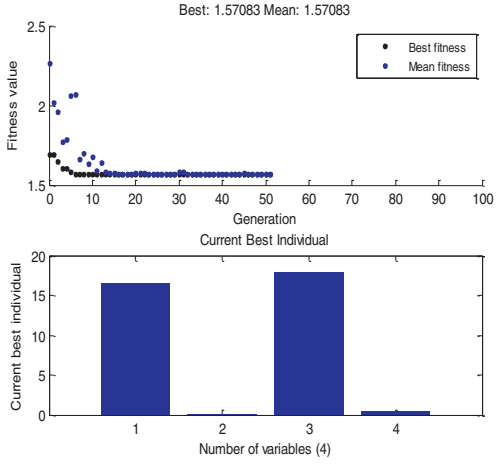

Fig. 13. The third joint: the objective values of different generations and the current optimized values.

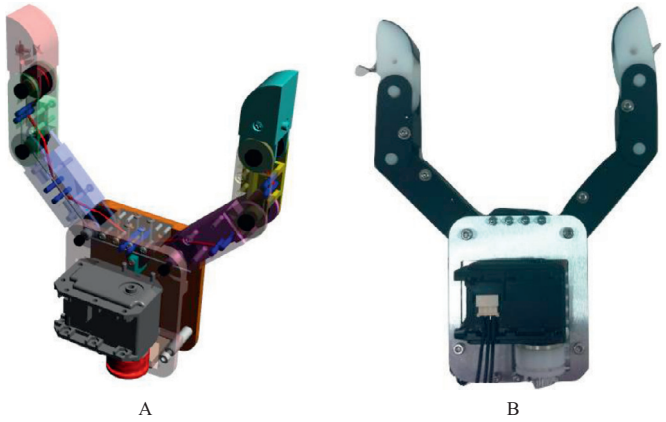

Fig. 14. The designed CAD model (A) and the prototype gripper (B).

the gripper can steadily grasp objects with the size range from 102 mm (the diameter of a cup) to 8 mm (the diameter of a pen). Specifically, the gripper picks up 38 objects successfully while a business card and a coin cannot be grasped with success since the contact position between the fingers and the object is higher than the height of the object. The real application cases are presented in Fig. 15. The gripper can perform stable enveloping grasps when the first phalanges touch the object to be stopped such that the second and third joints can flex to enclose the object. If the first and second phalanges are not blocked by the object, the gripper can execute a fingertip grasp by the distal phalanges closing in the opposite direction. As well, the gripper can passively adapt to the shape for grasping objects with irregular shapes due to the compliant characteristics of the under-actuated gripper with TDMs.

8. Conclusion

Geometric parameters of a two-finger gripper driven by TDMs are studied in this work by extracting a mathematical model of the force/torque transmission between an active force and contact forces based on the geometric analysis. In addition, a mathematical model is presented to obtain the transmission efficiency of the tension force when a tendon wraps a joint mandrel by the geometric relations. Genetic Algorithm is applied to optimizing the dimension of the gripper and the tendon routes. Specifically, we construct the two genetic-based fitness functions to be optimization objectives based on the grasping stability and the efficiency of the force transmission. The geometrically optimal approach provided by us has the characteristics of the versatility and can also be referred to optimizing most of the under-actuated robotic gripper with TDMs. We have validated this presented method by constructing an under-actuated gripper with TDMs depending on the optimized results and performing the practical experiments. In particular, the gripper can realize the stable grasps for a wide range of objects in household and office environments, and adapts to the shape of the grasped object because of the under-actuated mechanism.

Fig. 15. The practical grasping cases.

Future works would extend the optimization to the 3-dimension space. The thickness of the palm and phalanges and the fingertip shape will be explored and optimized, which allows an under-actuated tendon-driven robotic gripper to perform a stable grasp.

References

[1] S.C. Jacobsen, J.E. Wood, D. Knutti, K.B. Biggers, The UTAH/MIT dextrous hand: work in progress, Int. J. Rob. Res. 3 (1984) 21–50.
[2] H. Kobayashi, K. Hyodo, D. Ogane, On tendon-driven robotic mechanisms with redundant tendons, Int. J. Rob. Res. 17 (1998) 561–571.
[3] L. Birglen, T. Laliberté, C.M. Gosselin, Underactuated Robotic Hands, 40, Springer, 2007.
[4] N. Rojas, R.R. Ma, A.M. Dollar, The GR2 gripper: an underactuated hand for open-loop in-hand planar manipulation, IEEE Trans. Rob. 32 (2016) 763–770.
[5] A. Hassan, M. Abomoharam, Modeling and design optimization of a robot gripper mechanism, Rob. Comput. Integr. Manuf. 46 (2017) 94–103.
[6] J. Ölvander, M. Tarkian, X. Feng, Multi-objective optimisation of a family of industrial robots, in: Multi-objective Evolutionary Optimisation For Product Design and Manufacturing, Springer, 2011, pp. 189–217.
[7] T. Laliberté, C.M. Gosselin, Simulation and design of underactuated mechanical hands, Mech. Mach. Theory 33 (1998) 39–57.
[8] G.A. Kragten, F.C. Van der Helm, J.L. Herder, A planar geometric design approach for a large grasp range in underactuated hands, Mech. Mach. Theory 46 (2011) 1121–1136.
[9] L. Birglen, C.M. Gosselin, Kinetostatic analysis of underactuated fingers, IEEE Trans. Rob. Autom. 20 (2004) 211–221.
[10] T. Laliberté, C.M. Gosselin, Simulation and design of underactuated mechanical hands, Mech. Mach. Theory 33 (1998) 39–57.
[11] R.V. Rao, G. Waghmare, Design optimization of robot grippers using teaching-learning-based optimization algorithm, Adv. Rob. 29 (2015) 431–447.
[12] S. Hirose, Y. Umetani, The development of soft gripper for the versatile robot hand, Mech. Mach. Theory 13 (1978) 351–359.
[13] M. Zecca, G. Cappiello, F. Sebastiani, S. Roccella, F. Vecchi, M. Carrozza, et al., Experimental analysis of the proprioceptive and exteroceptive sensors of an underactuated prosthetic hand, Proceeding of the ICORR 2003 (The Eighth International Conference on Rehabilitation Robotics), 2003.
[14] A.M. Dollar, R.D. Howe, The highly adaptive SDM hand: design and performance evaluation, Int. J. Rob. Res. 29 (2010) 585–597.
[15] M. Ciocarlie, F.M. Hicks, R. Holmberg, J. Hawke, M. Schlicht, J. Gee, et al., The velo gripper: a versatile single-actuator design for enveloping, parallel and fingertip grasps, Int. J. Rob. Res. 33 (2014) 753–767.
[16] M. Ciocarlie, P. Allen, A constrained optimization framework for compliant underactuated grasping, Mech. Sci. 2 (2011) 17–26.
[17] T. Nishimura, K. Mizushima, Y. Suzuki, T. Tsuji, T. Watanabe, Variable-grasping–mode underactuated soft gripper with environmental contact-based operation, IEEE Rob. Autom. Lett. 2 (2017) 1164–1171.
[18] J. Krahn, F. Fabbro, C. Menon, A soft-touch gripper for grasping delicate objects, IEEE/ASME Trans. Mechatron. (2017).
[19] L.-W. Tsai, J.-J. Lee, Kinematic analysis of tendon-driven robotic mechanisms using graph theory, J. Mech. Transm. Autom. Des. 111 (1989) 59–65.
[20] J.-J. Lee, L.-W. Tsai, The structural synthesis of tendon-driven manipulators having a pseudotriangular structure matrix, Int. J. Rob. Res. 10 (1991) 255–262.
[21] Y.-J. Ou, L.-W. Tsai, Kinematic synthesis of tendon-driven manipulators with isotropic transmission characteristics, J. Mech. Des. 115 (1993) 884–891.
[22] R. Ozawa, H. Kobayashi, K. Hashirii, Analysis, classification, and design of tendon–driven mechanisms, IEEE Trans. Rob. 30 (2014) 396–410.
[23] Y. Qin, K. Zhang, J. Li, J.S. Dai, Modelling and analysis of a rigid–compliant parallel mechanism, Rob. Comput. Integr. Manuf. 29 (2013) 33–40.
[24] R. Datta, S. Pradhan, B. Bhattacharya, Analysis and design optimization of a robotic gripper using multiobjective genetic algorithm, IEEE Trans. Syst. Man Cybern. 46 (2016) 16–26.
[25] S.B. Backus, A.M. Dollar, An adaptive three-fingered prismatic gripper with passive rotational joints, IEEE Rob. Autom. Lett. 1 (2016) 668–675.
[26] M. Ciocarlie, F.M. Hicks, S. Stanford, Kinetic and dimensional optimization for a tendon-driven gripper, in: Robotics and Automation (ICRA), 2013 IEEE International Conference on, 2013, pp. 2751–2758.
[27] A.M. Dollar, R.D. Howe, Joint coupling design of underactuated hands for unstructured environments, Int. J. Rob. Res. 30 (2011) 1157–1169.
[28] J.M. Inouye, F.J. Valero-Cuevas, Anthropomorphic tendon-driven robotic hands can exceed human grasping capabilities following optimization, Int. J. Rob. Res. (2013) 0278364913504247.
[29] C. Gosselin, F. Pelletier, T. Laliberte, An anthropomorphic underactuated robotic hand with 15 dofs and a single actuator, in: Robotics and Automation, 2008. ICRA 2008. IEEE International Conference on, 2008, pp. 749–754.
[30] T. Treratanakulwong, H. Kaminaga, Y. Nakamura, Low-friction tendon-driven robot hand with carpal tunnel mechanism in the palm by optimal 3D allocation of pulleys, in: 2014 IEEE International Conference on Robotics and Automation (ICRA), 2014, pp. 6739–6744.
[31] J.M. Inouye, J.J. Kutch, F.J. Valero-Cuevas, A novel synthesis of computational approaches enables optimization of grasp quality of tendon-driven hands, IEEE Trans. Rob. 28 (2012) 958–966.
[32] M. Russo, M. Ceccarelli, B. Corves, M. Hüsing, M. Lorenz, D. Cafolla, et al., Design and test of a gripper prototype for horticulture products, Rob. Comput. Integr. Manuf. 44 (2017) 266–275.
[33] B. Alexander, K. Viktor, Proportions of hand segments, Int. J. Morphol. 28 (2010) 755–758.
[34] I.M. Bullock, T. Feix, A.M. Dollar, Analyzing human fingertip usage in dexterous precision manipulation: implications for robotic finger design, in: Intelligent Robots and Systems (IROS 2014), 2014 IEEE/RSJ International Conference on, 2014, pp. 1622–1628.
[35] M. Mitchell, An Introduction to Genetic Algorithms, MIT press, 1998.